Fuel Processing Technology 242 (2023) 107634

Contents lists available at ScienceDirect

Fuel Processing Technology

journal homepage: www.elsevier.com/locate/fuproc

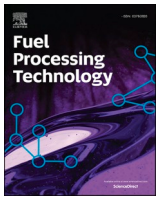

Bio-hydrogen and valuable chemicals from industrial waste glycerol via catalytic aqueous-phase transformation

A.J. Reynoso [a], J.L. Ayastuy [a,*], U. Iriarte-Velasco [b], M.A. Gutiérrez-Ortiz [a]

[a] Department of Chemical Engineering, Faculty of Science and Technology, University of the Basque Country UPV/EHU, Sarriena S/N, 48940 Leioa, Spain
[b] Department of Chemical Engineering, Faculty of Pharmacy, University of the Basque Country UPV/EHU, Paseo de la Universidad, 7, 01006 Vitoria, Spain

ARTICLE INFO

Keywords:
APR
Cobalt aluminate
Glycerol
Bio-hydrogen
Methanol
Acetic acid

ABSTRACT

Waste glycerol obtained as by-product of biodiesel production has been submitted to a sequential physico-chemical treatment in order to make it suitable for continuous Aqueous-Phase Reforming (APR) in a tubular reactor. Special focus was given to the impact of impurities. APR was performed using 0.3%Pt/$CoAl_2O_4$ catalyst, at 260 °C and 50 bar within WHSV range 6–55 h^{-1} to cover whole conversion ranges. Glycerol conversion and yield to hydrogen reached 99.7% and 45.4%, respectively at WHSV = 6 h^{-1}. The liquid product distribution strongly varied with glycerol conversion, maximum C-yield to 1,2-propylene glycol was attained in the 60–90% glycerol conversion range. APR of methanol and acetic acid aqueous feedstreams were investigated independently. It was concluded that acetic acid exerts a negative influence on catalyst stability since glycerol conversion decreased by 41% after 5 h TOS. Extensive characterization of fresh and exhausted catalysts revealed strong Co leaching, especially for acetic acid APR, oxidation of metals, and carbonaceous deposits. The basis for the regeneration of the spent catalyst, consisting of a reductive treatment at 500 °C, has been established. This work is expected to have significant implications for the development of APR technology for crude glycerol from biodiesel industry.

1. Introduction

The environmental concern of using fossil fuels makes imperative to develop clean and energy-efficient technologies for producing sustainable energy and chemicals. The use of biofuels such as biodiesel can reduce the short-term greenhouse gas emissions, reason for which its use has been driven by public policies [1]. Industrial biodiesel manufacturing consists on basic or acid catalyzed transesterification of free fatty acids (FFA) which produces glycerol as co-product, ca. 1 kg glycerol per 10 kg biodiesel [2]. The recent rapid growth of the biodiesel production has generated glycerol surplus that exceeds the current market demand. This crude glycerol is usually handled as waste, and causes an environment concern. Crude glycerol usually contains impurities such as methanol, ethanol, soaps, salts, FFAs, fatty acid methyl esters (FAMEs), glycerides and ash. Since purification to higher grade glycerol is economically unfeasible [3,4], valorization by producing energy and value-added chemicals is an economically promising alternative with a positive environmental impact [5,6]. For this reason, there exists an increased interest in seeking sustainable processes that allow the valorization of crude glycerol [7,8].

Aqueous-Phase Reforming (APR) is one of the most straightforward methods for glycerol valorization as it can deal with diluted aqueous feed streams. APR converts oxygenated hydrocarbons dissolved in water into hydrogen at relatively mild operation conditions. The obtained gaseous product is characterized by a low CO content, feasible to be directly used in PEM fuel cells [9–11]. Ideally, APR of polyols (C:O ratio = 1:1) comprises a first reforming step followed by the WGS reaction, the overall reaction being energy demanding.

Within the reaction mixture, side reactions such as CO hydrogenation (to form methane), C—O cleavage and hydrogenation, among others, can occur, which produce a wide range of gas and high value-added liquid products [12].

Much work has been carried out using synthetic glycerol as a model compound in APR [13–16], typically for H_2 production. To improve H_2 selectivity strategies such as in-situ adsorption of CO_2 in CaO are studied [17]. In a previous work [13], we suggested a plausible reaction pathway for the glycerol APR on the bifunctional dehydrogenation and dehydration/hydrogenation routes over the metal and the acid sites of the catalyst (Scheme 1, Supporting Information). In the "biomass-to-bioenergy" application, C—O bond hydrogenolysis gives rise to high

* Corresponding author.
E-mail address: joseluis.ayastuy@ehu.eus (J.L. Ayastuy).

https://doi.org/10.1016/j.fuproc.2022.107634
Received 25 October 2022; Received in revised form 20 December 2022; Accepted 22 December 2022
Available online 28 December 2022

value-added liquids, such as propylene glycol. Methanol APR has attracted particular interest in the last years as it contains the highest H: C ratio (4:1) among alcohols [18–20]. Using atomically dispersed Pt anchored on porous nanorods of ceria, H_2 can be generated at such a low temperature as 120 °C [21]. Methanol is also found in most crude glycerol streams from the transesterification process and can affect the glycerol APR [22].

Acetic acid is present in most of the aqueous streams derived from biomass and can represent up to 10–20 wt% of the aqueous fraction of pyrolysis oil [23]. Ideally, one mole of acetic acid can yield a maximum of four moles of H_2 (Eq. (1)).

$$CH_3COOH + 2H_2O \rightarrow 4H_2 + 2CO_2 \quad (1)$$

Acetic acid APR has been less investigated than the other two alcohols. The presence of a methyl group not activated by an hydroxyl one makes it more resistant to reforming reactions [24–27]. Consequently, higher temperatures are required for APR, and very low hydrogen yields are obtained. An additional operational difficulty is the catalyst deactivation by metal leaching promoted by the substrate acidity [26].

The catalyst stability in liquid-phase biomass treatments is challenging [28]. Among the different deactivation causes, the presence of organic acids in the reaction medium should be considered since it would hasten the metal leaching [29]. Catalyst poisoning and reactor clogging associated to inorganic salts and the inhibition of catalytic activity by competitive adsorption of organic impurities can also deactivate the catalyst [30,31]. There are limited works dealing with crude glycerol APR in a continuous reactor. Hydrogen production by feeding synthetic glycerol versus feeding crude glycerol on Pt-based catalyst was compared [32,33]. They found that production of hydrogen from crude glycerol was significantly lower than from the synthetic feedstock. Moreover, the yield to hydrogen rapidly decreased with time on stream, which was attributed to the presence of inorganic salts. Remón et al. [34,35] studied the effect of impurities (methanol, acetic acid, KOH, NaOH, acetic acid, sulfuric acid and phosphoric acid) in the APR of a 30 wt% synthetic glycerol/water feedstock over Ni-based catalyst. They found that Ni-leaching increased under acidic conditions, while KOH promoted hydrogen production. Similarly, other works carried out in batch reactor confirmed the negative effect of acetic acid and methanol impurities in the APR of glycerol over non-noble metal-based catalytic systems, which caused a significant decrease on the conversion to gas [29].

Most studies with crude glycerol are conducted in a batch reactor [29,31] being scarce the studies carried out in continuous fix bed reactors. Most of them evaluate the effect of the impurities under fixed operational conditions [33,35]. However, the product distribution greatly varies with the glycerol conversion, so it is crucial to ascertain the product distribution over a wide range of crude glycerol conversion values. The studies that deal with the effect of impurities in tubular reactors use synthetic mixtures, leaving aside the effect of other minor impurities (i.e. fatty acids, salts, etc.).

Given this background, this work fills the above-mentioned gaps regarding the APR of purified crude glycerol in continuous fix bed reactors. The main objective of the work is to gain knowledge on the continuous APR processing of glycerol streams. The product distribution for a wide range of conversion values and the effect of impurities (methanol and acetic acid) on the catalyst durability are studied. Moreover, an appropriate purification protocol for obtaining a glycerol feedstock suitable for continuous processing is established. In addition, a thorough characterization of the exhausted catalyst is conducted in order to establish the basis for its regeneration. For the APR runs, Pt supported on cobalt aluminate catalyst was chosen based in our previous work [36], where it showed high activity and stability in the APR of synthetic glycerol.

2. Experimental section

2.1. Crude glycerol analysis and purification process

The physicochemical characteristics of the biodiesel-derived waste crude glycerol depend on the raw material and the used synthesis route (i.e. use of base or acid catalysts; purification methods) [37]. An aqueous solution of waste glycerol (in advance referred "as received") was obtained from a local biodiesel plant (Bionor Berantevilla S.L., Spain). The presence of free fatty acids in the crude glycerol, made unfeasible the continuous processing in our experimental set-up due to pipe and bed clogging. Therefore, crude glycerol solution was submitted to a physico-chemical pretreatment before being treated in reactor.

The first stage of purification consisted on a saponification reaction in order to convert the free fatty acids into soaps. The saponification was carried out by addition of NaOH 2 M to the "as received" glycerol. The mixture was maintained under constant stirring at 60 °C for 30 min until pH 12.0 was reached. Then, the solution was settled overnight until complete separation of the two phases, and finally filtered. The soaps were discarded and the filtered fraction (in advance called "treated glycerol") neutralized with concentrated acetic acid. As a reference, a 10 wt% glycerol (PanReac 99.5% purity) aqueous solution (called "synthetic") was prepared.

Several physico-chemical properties were measured for the "as received", "treated" and "synthetic" glycerol samples. Density of each solution was determined with a pycnometer at room temperature by measuring the volume and weight of the sample. Viscosity of solutions at room temperature was measured by a RM180 Rheomat (Mettler Toledo) viscosimeter. The ash content was determined according to ISO 2098:1972 method [38]. The chemical composition of the obtained ash was determined by Wavelength Dispersive X-ray Fluorescence (WDXRF) technique (AXIOS, Analytical) employing the fusion method.

The content of glycerol and methanol was analyzed by HPLC using refraction index detector (Waters 616, Hi-Plex H column). The organic fraction of each sample was analyzed by GC–MS using a derivatization method. First, 170 μg of sample were saponified by addition of 2 mL KOH (2 M) and then acidified with HCl (2 M). The organic fraction was extracted with petroleum ether. Thereafter, the solvent was removed in a rotary evaporator, and the obtained organic fraction was derivatized with BSTFA (*N*,*O*-bis-(trimethylsilyl)trifluoroacetamide) and analyzed by GC–MS (HP-5MS column, He as carrier).

Attenuated total reflectance (ATR) infrared absorbance spectra of the liquid solutions were recorded at room temperature with a Fourier transform infrared (FTIR) spectrometer (Cary 600 Series, Agilent) equipped with a Linearized high-sensitivity MCT detector cooled with liquid-nitrogen and ATR accessory (Specac; SCF Diamond ATR Top Plate with a ZnSe crystal; incident angle, 45°). A drop of the solution was put on the crystal and an average of 52 scans were recorded at 4 cm^{-1} resolution in the 4000–350 cm^{-1} range.

2.2. Synthesis and characterization of the catalyst

Details on the synthesis of bimetallic 0.3Pt/CoAl catalyst can be found elsewhere [36]. Briefly, the support cobalt aluminate (nominal Co/Al mole ratio of 0.625) was synthesized by coprecipitation and then calcined at 500 °C. Pt was added by wet impregnation, to finally be calcined at 350 °C for 5 h. The bulk composition of the catalyst was assessed by ICP-AES after acid digestion. Metal leaching was determined from the ICP-MS analysis of the collected liquid product. The specific surface area and the main pore size were estimated by the BET and BJH methods, respectively, from the N_2 physisorption at 77 K in a Micromeritics TRISTAR II 3020 equipment. Previous to analysis, the sample was outgassed at 300 °C for 10 h in order to desorb impurities. XRD diffraction patterns of the catalysts were obtained on a PANalytical X'pert PRO diffractometer (CuKα radiation, λ = 1.5406 Å, graphite monochromator), with a step size of 0.026° (2θ) and a counting time of

2 s. The identification of the crystal phases was carried by comparison with International Centre of Diffraction Data (ICDD) database. The average crystallite size was calculated by Scherrer equation from the most intense peak X-line broadening.

The catalyst reducibility and cobalt speciation in the solids were studied by Temperature-Programmed Reduction (H_2-TPR) technique. The surface carbon deposits in exhausted catalyst was characterized and quantified by Temperature-Programmed Hydrogenation (TPH). The titration of Pt and Co metallic atoms at the catalyst surface was carried out by sequential pulse H_2 chemisorption at 40 °C. The surface acid/base characteristics of the catalyst were evaluated by means of NH_3 and CO_2 temperature programmed desorption, respectively. The skeletal isomerization of 3,3-dimethyl-but-1-ene (33DM1B) was used to characterize the Brønsted acid sites. Details of the employed protocols can be found elsewhere [13,36]. To further characterize the metallic function cyclohexane dehydrogenation was performed over reduced catalysts, in a fixed-bed reactor at 250 °C at atmospheric pressure, feeding mixture of anhydrous cyclohexane and hydrogen (1:3000 mol ratio). The gaseous products (benzene and cyclohexane) were online analyzed by GC-FID (column Al_2O_3-KCl, HP).

STEM Micrographs were taken with a FEI Titan Cubed G2 60–300 electron microscope equipped with a high-brightness and a Super-X EDX system under HAADF detector for Z contrast imaging (camera length of 185 mm). The sample was dispersed in ethanol and the suspension was kept for 15 min in an ultrasonic bath. Then, a drop of suspension was placed on a TEM copper grille (300 mesh) topped by a holey carbon film followed by vacuum drying. Particle size distribution was determined by measuring the diameter (d_i) of at least 300 particles (n_i) using ImageJ software. The average size of the nanoparticles was calculated from volume-to-surface ratio:

$$< d >= \frac{\Sigma n_i d_i^3}{\Sigma n_i d_i^2} \tag{2}$$

The Pt particles size uniformity is given as dispersity index (DI), calculated as follows [39]:

$$DI = \frac{\Sigma n_i \Sigma n_i d_i^4}{\Sigma n_i d_i \Sigma n_i d_i^3} \tag{3}$$

FTIR experiments were conducted on a Cary 600 Series FTIR apparatus with the catalyst powder diluted in a KBr pellet in the 500–4000 cm^{-1} region with a resolution of 4 cm^{-1}.

XPS measurements were carried out on a SPECS spectrometer with Phoibos 150 1DDLD analyzer. The spectrometer was previously calibrated using Ag $3d_{5/2}$ photoelectron line (BE = 368.26 eV), and Shirley background subtraction was employed. The catalyst was in-situ reduced at 600 °C in 20% H_2/Ar flow, for 1 h.

Raman spectra were taken on a Renishaw InVia Raman spectrometer coupled to a Leica DMLM microscope using a 514 nm laser. The Raman signal was acquired using 1800 lines/mm grating centered between 150 and 2000 cm^{-1}. For each spectrum, the acquisition time was 40 s, and 10 scans were accumulated at 10% of the maximum power of the laser.

2.3. Catalytic tests

The activity tests were conducted in a fixed-bed up-flow reactor (Microactivity Effi, PID Eng&Tech) according to the procedure described in a previous work [13]. All the tests were conducted at 260 °C and 50 bar. The catalyst mass (around 0.5 g) was kept constant while the feed stream flow was varied from 0.05 to 0.45 cm^3/min (WHSV = 6–55 h^{-1} range) in experiments with the "treated glycerol". This allowed investigation of the effect of the contact time on the catalytic performance. The APR runs using methanol and acetic acid were carried out at fixed WHSV of 24 h^{-1} (0.5 g of catalyst, 0.2 cm^3/min liquid flow). The absence of mass diffusion controls was assessed by the Weisz-Prater and Mears criteria (Table S1, Supporting Information).

The reaction products were separated by a Peltier device at 5 °C connected to a G/L separator. The gas phase products were on-line analyzed by an Agilent μGC using MS5A, PPQ, Al_2O_3-KCl columns. The liquid product was sampled hourly in 2 mL glass vials and off-line analyzed by an Agilent 6890 N GC-FID (HP-Wax bonded PEG column). External calibration method was used for the quantification of chromatographic analysis. Carbon concentration in the feed stream and the liquid effluent was determined by a Shimadzu TOC-L apparatus. The carbon balance was above 93% for all the experiments.

The conversion of reactants (X_{react}) and conversion of carbon to gas (X_{gas}) were calculated as follows:

$$X_{react}(\%) = 100 \times \frac{F_{react}^{in} - F_{react}^{out}}{F_{react}^{in}} \tag{4}$$

$$X_{gas}(\%) = 100 \times \frac{F_C^{gas}}{F_C^{in}} \tag{5}$$

where, $F_{react}^{in}$and F_{react}^{out} are the molar flow of reactant in the reactor inlet and outlet, respectively; $F_C^{gas}$and F_C^{in} are the molar flow of carbon atoms in gas stream and the carbon molar flow in the reactor inlet, respectively.

The gas phase was characterized by means of the selectivity (S_{H2}) and yield (Y_{H2}) to hydrogen, and selectivity to alkanes (S_{alk}) defined as follows:

$$S_{H2}(\%) = 100 \times \frac{2 \cdot F_{H2}^{out}}{F_H^{gas}} \tag{6}$$

$$Y_{H2}(\%) = 100 \times \frac{F_{H2}^{out}}{F_{H2}^{ideal}} \tag{7}$$

$$S_{alk}(\%) = 100 \times \frac{F_{alk}^{out}}{F_C^{gas}} \tag{8}$$

where, F_{H2}^{out}, F_H^{gas} and $F_C^{gas}$are the molar flow of H_2, H and C in gas-phase products at the reactor outlet, respectively; $F_{H2}^{ideal}$is the expected molar flow of H_2 in the absence of H_2-consumming reactions; $F_{alk}^{out}$is the molar flow of carbon atoms in alkanes at the reactor outlet.

Selectivity (S_i) and yield to liquid products (Y_i) were calculated by the following equations:

$$S_i(\%) = 100 \times \frac{F_i^{out}}{F_{react}^{in} - F_{react}^{out}} \tag{9}$$

$$Y_i(\%) = 100 \times \frac{F_i^{out}}{F_{react}^{in}} \tag{10}$$

where$F_i^{out}$is the molar flow of liquid product i at the reactor outlet.

Hydrogen production rate (rH2) was defined as the hydrogen flow at the reactor outlet per mass of catalyst. The specific reaction rate of glycerol (R_{Gly}) was calculated per gram of catalyst.

3. Results and discussion

3.1. Purification of waste glycerol

The most relevant physico-chemical properties of the "as received", "treated" and "synthetic" glycerol solutions are shown in Table 1. The "as received" glycerol solution was extremely acid (pH 1.1), whereas the "treated" and "synthetic" glycerol solutions were near neutral (pH 6.6–7.2). Both density and viscosity of "as received" and "treated" solutions were similar, and slightly higher than the "synthetic" solution (about 8% denser). The total carbon (TC) content decreased as follows: "as received" > "treated" > "synthetic". It could be explained by the fatty acids content, which decreased from 700 ppm in the "as received" glycerol solution to 20 and 15 ppm in the "treated" and "synthetic" solutions, respectively. In the "as-received" solution, stearic, oleic and linoleic species were the most abundant, accounting for 87% of the total

Table 1
Physico-chemical properties of "as received", "treated" and "synthetic" glycerol solutions.

	"As received"	"Treated"	"Synthetic"
Physical properties			
pH	1.1	7.2	6.6
Density (g/cm^3)	1.1112	1.1025	1.0234
Viscosity (mPa·s)	1.17	1.15	1.05
TC [a] (g/L)	84.0	55.5	39.9
Chemical composition			
Glycerol (wt%)	13.0	9.7	10.0
Methanol (wt%)	4.8	1.8	0
Acetic acid (wt%)	0	0.6	0
C8:0 (ppm)	6.4	3.6	3.4
C10:0 (ppm)	4.3	0.8	0.9
C12:0 (ppm)	6.9	0.7	0.7
C14:0 (ppm)	8.7	0.5	0.4
C16:0 (ppm)	49.5	0.7	1.0
C18:0 (ppm)	75.6	5.7	6.1
C18:1 (ppm)	259.8	0.9	n.d.
C18:2 (ppm)	271.0	4.1	n.d.
C18:3 (ppm)	16.0	2.9	1.6
Ash (wt%)	8.84	8.60	0.05

n.d.: not detected (Detection limit 0.2 ppm). Caprylic acid (C8:0); Capric acid (C10:0); Lauric acid (C12:0); Myristic acid (C14:0); Palmitic acid (C16:0); Stearic acid (C18:0); Oleic acid (C18:1); Linoleic acid (C18:2); Linolenic acid (C18:3).

[a] TC: Total Carbon.

fatty acid content. It is remarkable the high removal efficiency of most fatty acid species during the saponification step (removal efficiency from 81.4% to 99.6% for capric to oleic species, respectively). From results in Table 1, it seemed that short chain species were removed to a lesser extent. For instance, only 44% of the caprylic acid was readily removed. Its relative contribution to the total fatty acid content in the "treated" solution increased by around 20-fold. It is noteworthy that the removal of stearic acid was somewhat lower than that attained for similar chain species. Consequently, its relative contribution in the treated sample also increased, by around 3-fold.

The ash content (around 9 wt%) indicated the presence of inorganic materials from transesterification process. The ash content was similar in the "as received" and "treated" glycerol solutions (i.e. 8.6–8.8 wt%), and significantly lower in the "synthetic" solution (0.05 wt%). XRD pattern of crude bioglycerol ash (Fig. S1, Supporting Information) exhibited peaks attributable to carbonate, sulfate and phosphate salts which matched with the following: $Na_2CO_3{\cdot}H_2O$ (PDF 08–0448), $K_{0.67}Na_{1.33}SO_4$ (PDF 20–0926), Na_2SO_4 (PDF 24–1132) and Na_2HPO_4 (PDF 35–0735). The WDXRF chemical analysis of ash (Table S2, Supporting Information) revealed a high content of Na and S (above 20 wt %) and a considerable content in K (4–7 wt%). The presence of Na was attributed to the Na-based alkali used during the biodiesel processing, while S was likely due to acidification of crude bioglycerol during its purification stage at the industry, and consistent with its low pH level [40]. Excess SO_4^{2-} reacted with potassium ion from soap to form insoluble K_2SO_4. The content of other minor constituents further decreased upon saponification.

Fig. 1 shows the ATR-FTIR spectra of the "as received", "treated" and "synthetic" glycerol solutions, in addition to those from the methanol and acetic acid solutions (both at 10 wt%). All solutions presented a broad band in the 3700–2800 cm^{-1} range (not shown), typical of the stretching vibrations of the O—H bonds in hydroxyl group and water molecules [41]. This large band is very pronounced due to the high water content and therefore masks the typical peaks corresponding to asymmetric and symmetric CH_2 stretching mode, which can be observed in the spectra of pure compounds (Fig. S2, Supporting Information). In addition, a band centered at 1640 cm^{-1} emerged, which was due to stretching vibrations of the H-O-H bond.

Several peaks could be perceived in the 1300–950 cm^{-1} range, for

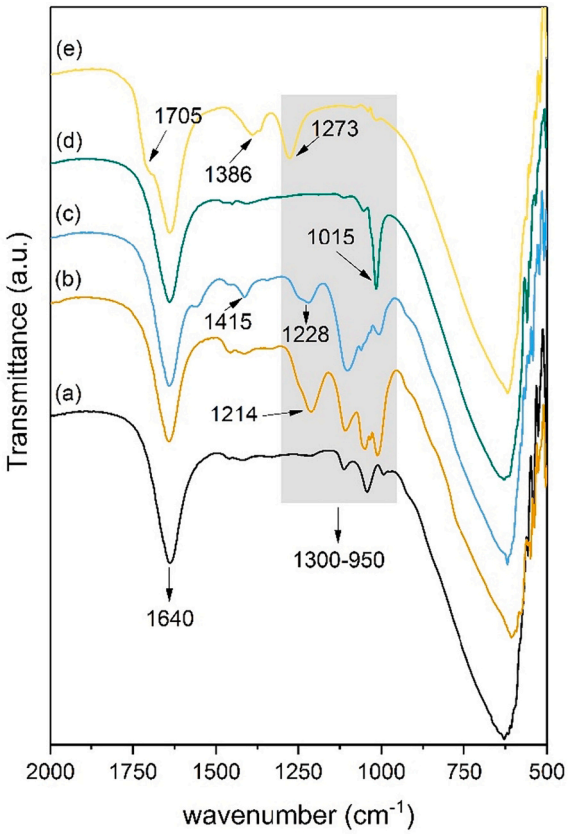

Fig. 1. ATR-FTIR absorption spectra for: (a) "synthetic" glycerol solution (10 wt%); (b) "as received" crude glycerol; (c) "treated" glycerol; (d) 10 wt% methanol aqueous solution; and (e) 10 wt% acetic acid solution.

the different glycerol solutions. The band at 1214 cm^{-1} observed in crude "as received" glycerol, characteristic of the hydrocarbon chain structures present in FAMEs [42], notably decreased after treatment. Likewise, the peak at around 1015 cm^{-1} showed a similar behavior. The latter peak is characteristic of methanol [43], therefore a marked reduction in methanol content in the "treated" solution could be deduced. Regarding the acetic acid solution, the most distinct band appeared at 1705 cm^{-1}, attributable to C═O stretching mode of carbonyl group, together with other bands at 1415, 1386 and 1273 cm^{-1}, corresponding to O—H and C—H bending and strong C—O stretching, respectively [44]. The increased intensity at around 1415 cm^{-1} in the treated assay reflected the presence of acetic acid in this sample, likely remaining after the neutralization process. Finally, a doublet at 1111 and 1050 cm^{-1} was observed for the "as received" and "treated" solutions, which could be assigned to the O – CH_2 – C asymmetric axial stretching [45].

3.2. Effect of WHSV on the APR of "Treated" bioglycerol

Preliminary APR runs with "as received" glycerol clogged the reactor after few minutes of operation, making necessary its pre-treatment before being processed. APR runs with "treated" bioglycerol were performed at 260 °C and 50 bar, by duplicate. Experimental data were collected at 1 h TOS. In all cases, the experimental error associated to the glycerol conversion was below 4%. WHSV variation in the 6–55 h^{-1} range gave glycerol conversions in the 99.7–14.3% range. As could be expected, the glycerol conversion decreased with spatial velocity. In the same line, carbon conversion to gas decreased with WHSV, as a consequence of insufficient contact time for the intermediate liquid products to undergo consecutive reforming reactions [46,47]. The analysis of the gas and liquid products indicated that the carbon contained in the

glycerol was converted into both gaseous and liquid products. Fig. 2 shows the selectivity of carbon atoms in the liquid products and in the gas phase products in the whole range of glycerol conversion. The specific reaction rate of glycerol conversion (R_{Gly}) was also calculated (Table S3, Supporting Information), which showed a volcano-type shape with maximum rate at c.a. 60% glycerol conversion.

Considering the mole ratio between the gas and liquid products (Gas/Liquid), obtained data revealed three characteristic regions. The first one, up to approximately 50% glycerol conversion, where the production of intermediate liquid compounds doubled that of the gaseous compounds (Gas/Liquid ratio varied in the 0.38–0.49 range). The high percentage of intermediate liquid products was clearly related to the established high feed rate, since at low contact times, the dehydration/dehydrogenation reactions prevailed [13].

In the X_{gly} = 50–90% range, the gas production steadily increased, with Gas/Liquid values in the 0.6–0.8 range. At almost complete glycerol conversion, Gas/Liquid reached up to 1.71, and X_{gas} achieved 63%. The observed behavior suggested that the reaction pathway might be tuned, by the WHSV, to approach the desired catalyst performance.

Fig. 3a depicts the most representative parameters of gas-phase products. Y_{H2} increased with glycerol conversion, reaching 45.4% at 99.7% glycerol conversion. Note that high conversion favored reforming reactions of the liquid intermediates, which produced hydrogen. Selectivity to hydrogen was high for the investigated 0.3Pt/CoAl catalyst (i.e. $S_{H2} > 60\%$) in the whole glycerol conversion range, what is comparable to other Co- and Pt-containing catalysts used with synthetic glycerol-water feed streams [48]. Selectivity to methane (S_{CH4}), another valuable product in the gas phase, varied between 10 and 20% (not shown). However, methane was not the most abundant alkane in the X_{gly} range 45–60%. Under such operational regime, selectivity to alkanes (S_{alk}), which accounted for the sum of methane, ethane, and propane, showed a volcano-type dependence with its highest values (S_{Alk} = 42–51%) at intermediate glycerol conversion values (i.e. X_{Gly} = 40–60%). In the APR process, small alkanes could be formed from the scission of C—C bonds and subsequent hydrogenation reactions [49]. For instance, ethanol can undergo dehydration and subsequent hydrogenation to form ethane. Therefore, the high availability of liquid products might increase production of C_{2+} gases. Interestingly, at the highest glycerol conversion, methane was, by far, the main alkane species, accounting for above 80% of all alkanes).

Fig. 3b depicts the product distribution in the gas phase. As observed, hydrogen was the main gaseous product in the whole glycerol conversion range, followed by carbon dioxide, alkanes and, in much lesser extent, carbon monoxide (in all cases below 0.01%). The lowest H_2 molar concentrations (i.e. ~43–50%) were obtained at low glycerol conversions ($X_{Gly} < 20\%$. H_2/CO_2 ratio was around 1 at such low conversion values, and smoothly increased with glycerol conversion, up to around 2 at 50% X_{Gly}. Above this conversion, H_2/CO_2 ratio smoothly decreased to below 1.7. The existence of a maximum in H_2/CO_2 ratio coincided with a maximum of S_{Alk}. Taking into account that, for the ideal APR of glycerol, the H_2/CO_2 molar ratio is 2.3, in-situ consumption of a fraction of the produced H_2 could be anticipated, in reactions such as production of alkanes or hydrogenolysis. Indeed, the lowest H_2/CO_2 ratio coincided with the lowest Gas/Liquid product ratio.

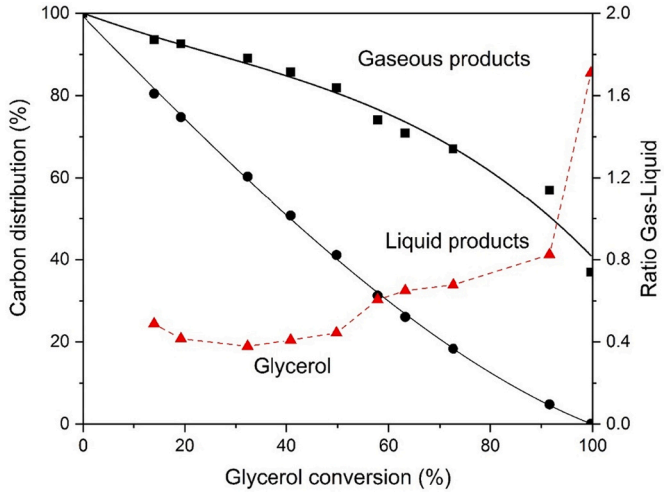

Fig. 2. Carbon selectivity (continuous lines) and Gas/Liquid products mole ratio (dashed line) as a function of glycerol conversion. Feedstream: "treated" bioglycerol. Reaction conditions: 260 °C/50 bar. Maximum error in glycerol conversion below 4%.

Regarding the liquid products, hydroxyacetone, 1,2-propylene glycol, propanoic acid, ethanol and ethylene glycol were the main species. Others, like acetone and 1-propanol, showed much lower yields. Interestingly, the yield of the liquid species strongly depended on the glycerol conversion, as illustrated in Fig. 4.

According to reaction paths in Scheme 1 (Supporting Information), hydroxyacetone is the primary product of glycerol dehydration and precursor of both 1,2-propylene glycol and propanoic acid. All these C_3 compounds presented an increasing trend with the conversion of glycerol. In the low X_{Gly} region, the highest yield corresponded to propanoic acid ($Y_{propanoic\ acid}$ = 5%). However, at above 50% glycerol conversion, the highest yield corresponded to 1,2-propylene glycol (12.5%). This fact could be ascribed to the enhanced capacity of our catalyst for hydrogenation of liquid intermediates which would be favored due to an increased partial pressure of hydrogen in the reactor accompanied by an increased production of liquid intermediates [50]. Interestingly, the yields of the above mentioned three products drastically decreased at almost complete glycerol conversion, with the concomitant increase of 1-propanol. Similar trend was observed for the yields to ethanol and ethylene glycol. These latter species were, however, formed at much lesser concentrations (i.e. 3.5 times lower, maximum yield 4.7% and 3%, respectively). Other products were only detected at high glycerol conversions; acetone (at $X_{gly} \geq 60\%$), propanal and 1-propanol (at $X_{gly} \sim 100\%$). It must be noted that these were produced from successive dehydration and hydrogenation reactions [13]. Their formation was therefore consistent with the high catalytic activity.

Noteworthy, the yields to methanol and acetic acid, impurities present in "treated" glycerol feed stream, decreased with glycerol conversion, what suggested that both compounds were reformed to some extent, and could contribute to produce additional hydrogen. Moreover, the yield to methanol decreased more sharply than the yield to acetic acid, likely due to the easy activation of C—H bonds of methanol by adjacent OH, what does not occur for acetic acid. Our results were consistent with the low reactivity of acetic acid in liquid phase [51]. Several authors have reported the impact of these compounds on the APR performance [18,25,52,53]. In general, it is agreed that full reforming of acetic acid to H_2 and CO_2 is difficult to attain and that a mixture of CO_2 and CH_4 is obtained [25]. The sharp drop in the H_2/CO_2 ratio at around 60% glycerol conversion could be explained by the accumulation of ethanol in the reaction mixture, which selectivity towards H_2 is hindered by the presence of the non-activated methyl group, thus being transformed to CH_4 [52]. This behavior is in line with the increasing trend of SCH_4 at above 60% glycerol conversion.

The carbon selectivity of the main liquid products was calculated. The evolution of the carbon selectivity throughout the APR of glycerol is shown in the Supporting Information (Table S3). At the lowest conversion, the highest values corresponded to hydroxyacetone and propanoic acid (9.35% and 10.2%, respectively), followed by 1,2-propylene glycol (5.9%), ethylene glycol (2.6%) and ethanol (1.1%). As a general trend, carbon selectivity among the aqueous products increased as the APR reaction proceeded, except for hydroxyacetone (which slightly decreased to 8.2%) and propanoic acid, which not varied. The highest increase was noted for 1,2-propylene glycol (up to 16.3%) and ethanol (4.8%).

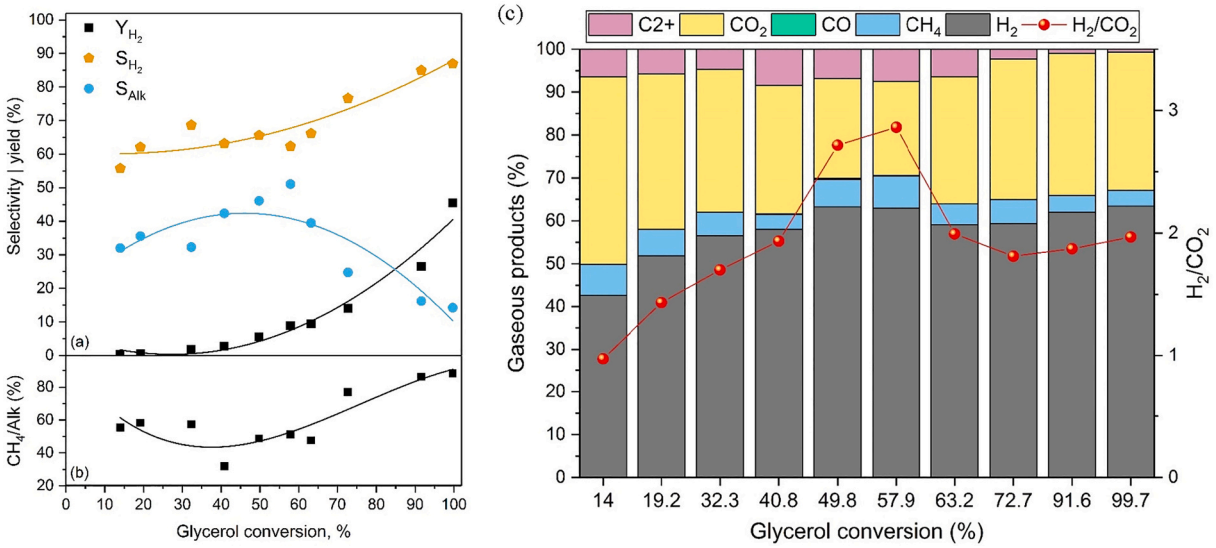

Fig. 3. Variation with glycerol conversion of (a) Selectivity to H_2 and alkanes, and H_2 yield; (b) Percentage of CH_4 respect to all alkanes; (c) Distribution of gas-phase products.

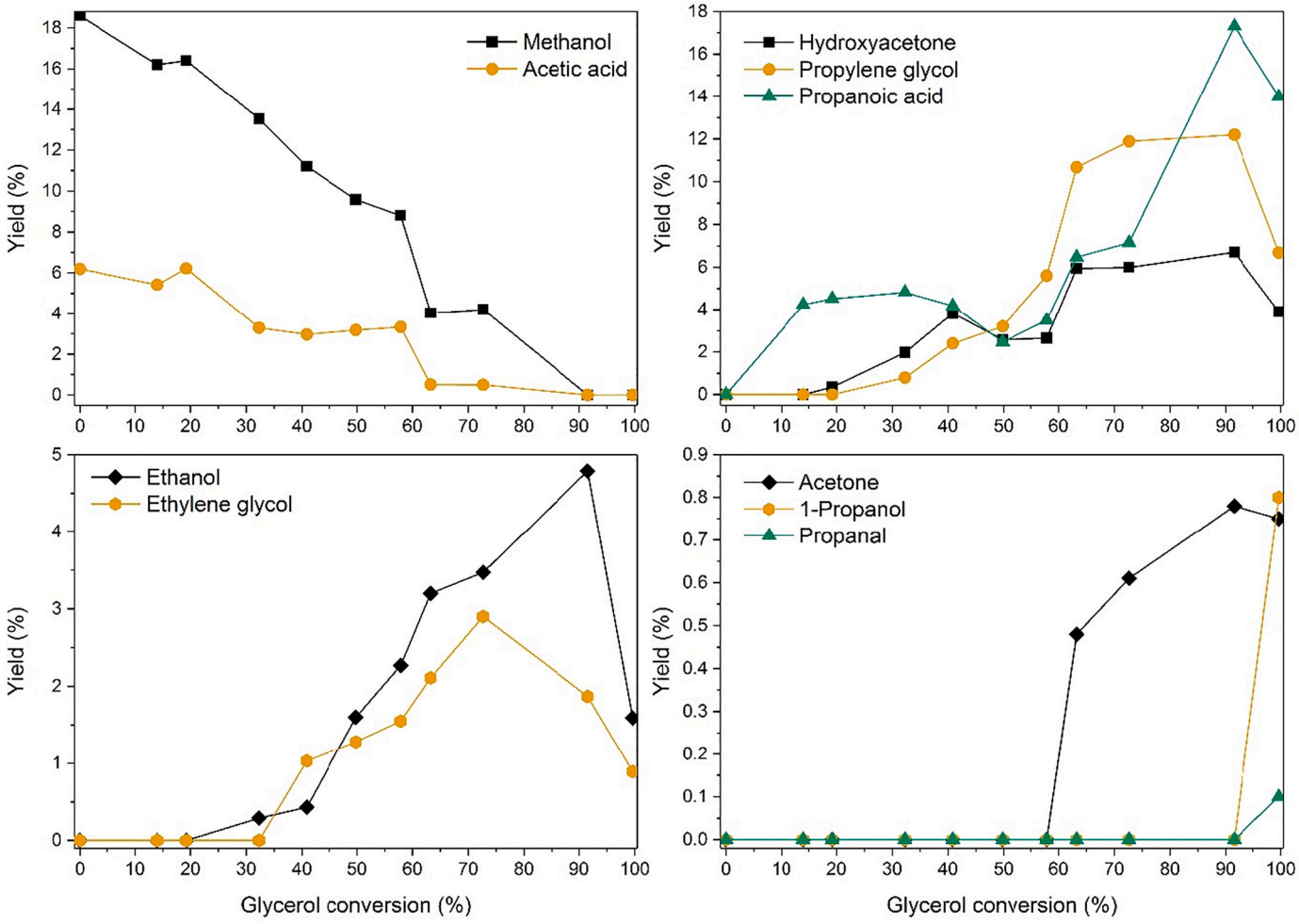

Fig. 4. Yield of liquid products as a function of glycerol conversion for "treated" glycerol feed stream.

3.3. *Effect of impurities in the feedstock*

Additional APR runs were carried out using aqueous solutions of methanol and acetic acid (separately) as feedstock, and compared to results obtained in the APR of "treated" glycerol. Some of the obtained reaction indices are shown in Fig. 5.

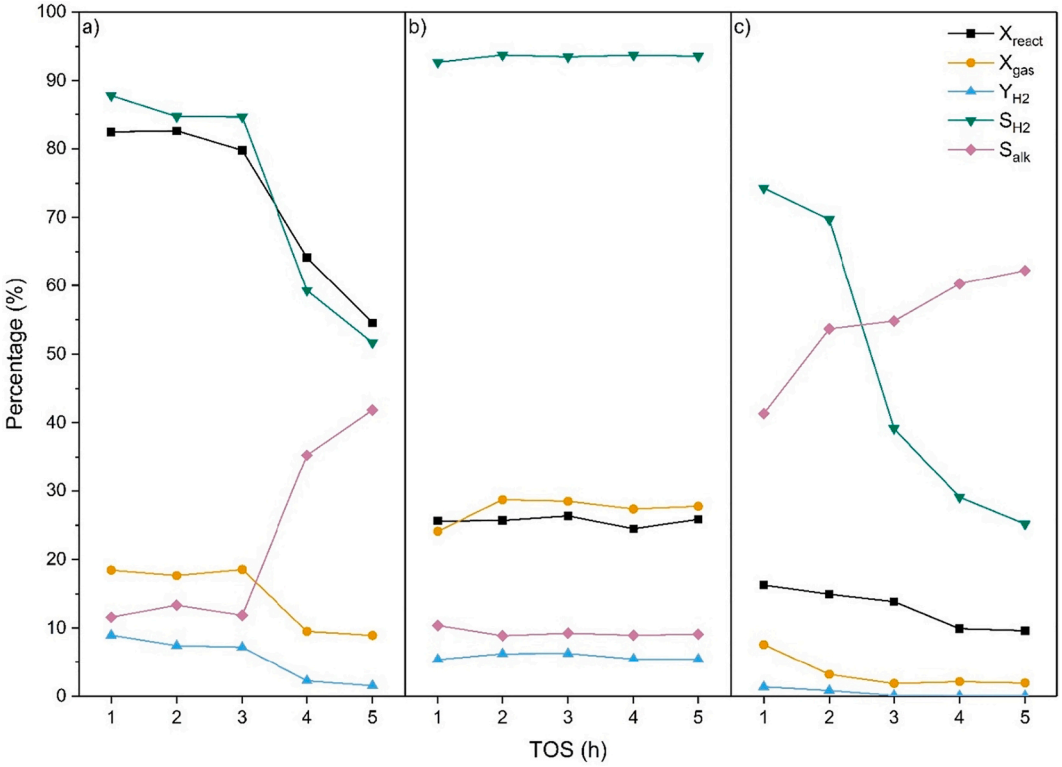

Fig. 5. Aqueous-phase reforming of a) "treated" glycerol, b) methanol (10 wt% aqueous solution), and c) acetic acid (10 wt% aqueous solution). Reaction conditions: 260 °C, 50 bar and WHSV of 24.5 h^{-1}.

During the APR of "treated" glycerol the conversion remained quite stable during the first 3 h TOS (i.e. $X_{gly} \approx 82\%$, $r_{H2} = 242.4$ $\mu mol_{H2}/min \cdot g_{cat}$). Afterwards, after 5 h TOS, the activity abruptly declined (i.e. $X_{gly} \approx 55\%$), with around five-fold decrease in H_2 production rate ($r_{H2} = 51.7$ $\mu mol_{H2}/min \cdot g_{cat}$). Consequently, carbon conversion to gas, and yield and selectivity to hydrogen also decreased, whereas, selectivity to alkanes increased.

These results were consistent with previous results, i.e., selectivity towards alkanes spiked at intermediate (40–65%) glycerol conversions. This behavior diverged with respect to that obtained with synthetic glycerol, where very high stability was noticed [36].

In the APR of methanol, the activity of 0.3Pt/CoAl catalyst remained stable throughout 5 h TOS with a moderate methanol conversion ($X_{methanol} \approx 25\%$). The considerably lower APR activity for methanol as compared to glycerol, could be attributed to the higher activation energy barrier for methanol reforming [54] in comparison to the high functionalized glycerol molecule. Interestingly, methanol was fully converted into gaseous products (i.e. $X_{gas} \approx X_{methanol}$), in line with other authors [18,55]. All reaction indices were stable, with H_2 yield (5%), S_{H2} (93%) and S_{Alk} (10%, CH_4 only). The H_2 production rate stabilized at 230 $\mu mol_{H2}/min \cdot g_{cat}$. These results were encouraging compared to others reported in the literature (24.5 h^{-1} vs < 4 h^{-1}) taken into account the high WHSV used in our experiments [56].

Results of the APR of acetic acid indicated that it showed the lowest conversion among all the feed streams, pointing its high stability in aqueous phase. Conversion at 1 h TOS was 16.3%, and monotonically decreased with TOS (10% at 5 h TOS). Accordingly, X_{gas} decreased steeply in the first 3 h TOS (75% decay) and then more gently. No liquid products were detected in the whole reaction period. Regarding rH_2, it was the lowest among all the freestreams, and passed from 2.2 to 0.8 $\mu mol_{H2}/min \cdot g_{cat}$ from 3 h TOS to 5 h TOS. Clearly, APR reactivity of acetic acid was much lower than those observed in the APR of "treated" glycerol and methanol. Selectivity to H_2 dropped by 66% over the first 5 h TOS, while production of methane (the only alkane detected) increased by 50.6%. The high values of S_{Alk} were in line with literature [30,52,57].

Several authors have reported low APR reactivity of acetic acid [25–27,52,58], and attributed to the presence of a methyl group not activated by a hydroxyl one. Methane and carbon dioxide were reported as the main species among the gaseous products.

Although methanol and acetic acid possess great potential for catalytic reforming, when present as impurities, they can lead to fast catalyst deactivation. Especially the latter, which can exert a negative effect on the catalytic behavior [25]. Alternatively, acidification could be done with mineral acids (sulfuric, hydrochloric, phosphoric acid). Nevertheless, the corrosive nature of these acids and the non-biodegradability of the salts generated could be a real operational problem [59].

Our results revealed that both impurities influenced negatively the glycerol conversion and the specific reaction rate (Table S4, Supporting Information), as for similar WHSV values, the obtained X_{Gly} and specific reaction rate (R_{Gly}) were significantly lowered as compared to APR of synthetic glycerol. The fact that no liquid products were produced during the APR of methanol and acetic acid suggests that APR of the treated glycerol could proceed through a similar reaction path to that of synthetic glycerol.

3.4. Characterization of fresh and exhausted catalysts

Table 2 summarizes the main physico-chemical characteristics of fresh 0.3Pt/CoAl catalyst (on its reduced form). The measured Pt content and the Co/Al mole ratio of the support were close to the nominal values. The available metallic cobalt area was 4-fold larger than that of platinum (2.01 vs 0.44 m^2_{Metal}/g_{cat}), due to the much higher Co content. However, in terms of bulk composition, the difference was much higher (bulk Co/Pt mole ratio $8.2 \cdot 10^4$), what suggested the existence of much larger metallic cobalt particles than those of platinum. The Pt dispersion calculated from H_2-chemisorption was 58%, which gave an average Pt particle size of 2.4 nm.

Table 2
Bulk composition, metallic area and surface chemistry of the reduced 0.3Pt/CoAl catalyst.

Pt loading[a] (wt%)	Co/Al[a] (at./at.)	S_{Pt}[b] ($m^2_{Pt^0}/g$)	S^0_{Co}[b] ($m^2_{Co^0}/g$)	D_{Pt} (%)	Basic sites density[c] ($\mu mol_{CO2}/m^2$)	Acid sites density[d] ($\mu mol_{NH3}/m^2$)	TOF dehydration[e] (s^{-1})	33DM1B isomerization activity[f] ($\mu mol_{33DM1B}/m^2h$)
0.29	0.634	0.44	2.01	58	1.16	0.56	2.29	85.6

[a] ICP-AES.
[b] H_2 chemisorption.
[c] CO_2-TPD.
[d] NH_3-TPD.
[e] Cyclohexane dehydrogenation.
[f] 33DM1B isomerization.

According to HAADF-STEM (Fig. S3, Supporting Information) the reduced catalyst consisted on very small and homogeneously distributed Pt nanoparticles and bigger nanoparticles of cobalt. Moreover, it was confirmed that Pt was mainly deposited onto Co-rich and Al-rich phases. The EDX mapping for Co suggested segregation of cobalt, while Al atoms presented a homogeneous chemical distribution. The mean particle size of Pt was 1.62 nm, with very narrow size distribution (DI = 1.02). This size was slightly lower than that calculated from H_2 chemisorption (2.4 nm) probably due to the lowering of hydrogen chemisorption as due to strong Pt—Co interactions. The average size of cobalt particles was 20.3 nm.

The activity (in terms of TOF) of 0.3Pt/CoAl catalyst in the cyclohexane dehydrogenation (model reaction) was 2.29 s^{-1}, indicating metallic sites with high intrinsic activity [60]. These metallic sites are known to be involved in the activation of the H_2 molecule for the hydrogenolysis reactions [61].

The density of acid and basic centres revealed the amphoteric nature of our 0.3Pt/CoAl catalyst, with a dominant basic character (twofold basic to acid sites density). The Brønsted sites were evaluated by the well known 33DMB1 isomerization reaction, which takes place through a pure protonic mechanism [62]. The measured isomerization activity (85.6 $\mu mol_{33DM1B}/m^2h$) was well below 200 $\mu mol_{33DM1B}/m^2h$, indicating a low contribution of Brønsted acid sites to the total acidity. Our results were in line with literature for cobalt aluminate spinels [63].

XPS was used to investigate the surface chemical composition and oxidation state of the atoms in the reduced form of the catalyst. Table S5 and Fig. S4 (Supporting Information) show the most relevant XPS parameters together with XPS survey spectra and high-resolution spectra of Co 2p, Al 2p and Pt $4d_{5/2}$. Survey spectrum essentially showed peaks from Co, Al, and O, while Pt was not observed due to its low content. Characteristic spin-orbit splitting of Co $2p_{3/2}$ and Co $2p_{1/2}$ levels could be observed, with the corresponding shake-up satellite peaks. The existence of such satellite peaks indicated the presence of Co^{2+}. Deconvolution of Co $2p_{3/2}$ and Co $2p_{1/2}$ peaks indicated the absence of Co^{3+} contributions. The peaks at 778.2 and 793.9 eV were attributed to metallic Co, while the peaks at 781.6 and 797.7 eV could be ascribed to Co^{2+} species. In addition, the satellite peaks at 786.0 and 803.4 eV corresponded to Co^{2+} [64]. The relative contribution of metallic Co atoms accounted for 46.9% of all cobalt. The very weak intensity peak of Pt^0 (at 314.0 eV) makes unfeasible its quantitative analysis.

Al 2p level binding energy was measured at 74.2 eV, which is typically ascribed to Al_2O_3 species [65]. In spite of the low platinum content, binding energies of the Pt $4d_{5/2}$ level could be observed at 314.0 eV, which corresponded to Pt^0. No other peaks for Pt were observed.

The Co/Al ratio at the surface of the catalyst (in its reduced form) was 0.184 what was notably lower than that (0.634) measured at bulk level, what indicated a surface enrichment in Al, as a consequence of the lower surface free energy of Al as compared to Co [66].

The specific surface area (S_{BET}), pore volume (d_{pore}) and the average pore size (V_{pore}) of the reduced and exhausted catalysts are displayed in Table 3, while the N_2 isotherms are plotted in Fig. S5, Supporting Information. All the catalysts (fresh reduced and spent in the APR of different substrates) showed type IV isotherms characteristic of mesoporous solids with H2 type hysteresis loop at high relative pressures, characteristic of disordered porous materials. Substantial textural changes, regardless of the substrate used, could be inferred. After methanol APR, d_{pore} and V_{pore} decreased by 42% and 29%, respectively. The decreasing trend in pore volume was similar for all the spent samples. However, S_{BET} showed a different behavior depending on the used feedstock. It increased after acetic acid APR; it decreased for the "treated" glycerol APR while it did not vary during APR of methanol. The increase in the specific surface area (in the case of acetic acid substrate) could be ascribed to the re-deposition of aluminium hydroxide on the catalyst surface. It is known that alumina hydroxylation can occur in hot water, it can be then leached and re-deposited onto the catalyst surface [67]. Such re-deposition phenomena could explain the fast activity decay of the catalyst during acetic acid APR, decorating the active metal sites.

The product liquid stream was analyzed and no Pt was detected whereas the measured Al concentration reflected an insignificant leaching (Al leaching <0.38%). Nonetheless, reforming under acid medium caused a considerable loss of cobalt (i.e. 19.7% acetic acid APR; 8.1% "treated" solution APR). Indeed, leaching remains as one of the main disadvantages of using transition metals for APR in acid media [26,30] which causes non-reversible deactivation.

XRD patterns of the reduced and used catalysts in the APR of different feedstocks (Fig. S6a, Supporting Information) presented typical diffraction peaks from spinel. Characteristic peaks of metallic cobalt were also detected. These were of much lower intensity in the spent catalysts what is consistent with the previously noted metal decoration during APR. No diffraction peaks from platinum species were detected,

Table 3
Physico-chemical properties of the reduced and spent 0.3Pt/CoAl catalyst.

Catalyst form	S_{BET}[a] (m^2/g)	d_{pore}[a] (nm)	V_{pore}[a] (cm^3/g)	d_{spinel}[b] (nm)	Leaching (wt%)		H_2 uptake ($mmol_{H2}/g_{cat}$)	
					Al	Co	TPR_{600}	$TPR_{600-950}$
Fresh Reduced	131	14.8	0.52	6.3	–	–	5.1[c]	2.2[c]
After Methanol APR	131	8.6	0.37	6.1	< 0.01	0.1	2.0	2.8
After Acetic acid APR	166	8.4	0.38	5.9	0.38	19.7	0.2	3.0
After "Treated" glycerol APR	93	13.2	0.39	5.7	0.06	8.1	3.1	1.4

[a] Nitrogen physisorption.
[b] XRD.
[c] Calcined form of solid.

as due to its high dispersion. The catalyst used in the APR of the so-called "treated" glycerol showed an additional peak at 34°, ascribed to sodium sulfate (PDF 24–1132), which could affect catalyst life time. This finding agreed with the XRD analysis of ashes (Fig. S1, Supporting Information). Finally, the diffraction peak at about 26° was indicative of graphitic carbon (PDF 00–056-0159), being more intense in the acetic acid APR-used catalyst.

The presence of carbonaceous material in spent catalysts was further investigated by Raman (Fig. S6b, Supporting Information). D-band (1340–1400 cm^{-1}, from defect structure like amorphous and defective carbon) was only visible for the catalyst after acetic acid APR. It was of much less intensity than G-band (1550–1600 cm^{-1}, from sp^2 hybridization, like graphite-like carbon), indicating the existence of poorly organized carbonaceous material. The low intensity of both bands suggested low amounts of deposits, in line with the XRD data of spent catalysts. Indeed, the established pressure, temperature and high WHSV values hinder the formation of carbonaceous material [13,68,69].

The FTIR spectra of the spent catalysts are also shown in Fig. S6c, Supporting Information. All the solids showed transmittance bands at around 575 and 660 cm^{-1}, attributed to the Co—O vibration modes in spinel structure [70]. For the spent catalysts, a strong band emerged at 1400 cm^{-1}, ascribable to O—H bending modes of organic compounds and water. Furthermore, two new bands arised for catalyst used in the APR of the "treated" glycerol; first, at around 1122 cm^{-1}, ascribed to the asymmetric stretching vibration of the SO_4^{2-} group [71] (in line with XRD results) and, second, at around 1012 cm^{-1}, ascribed to C═C bending modes of coke precursors [72]. The latter was visible for all the spent catalysts.

Reducibility of the solids was evaluated by H_2-TPR in two consecutive TPR runs. First, the solid was heated in H_2/Ar flow up to 600 °C and hold for 1 h, which simulated the in-situ reduction stage before the catalytic tests. The H_2 uptake in this step was named TPR_{600}. Then, the solid was cooled down to room temperature, and a second H_2-TPR analysis was carried out heating up to 950 °C. The H_2 uptake in this second run was named $TPR_{600/950}$. Both TPR profiles are displayed in Fig. 6, and the corresponding H_2 uptake values are given in Table 3. The peak assignment for the fresh catalyst in TPR_{600} was as follows: the low temperature peak (below 200 °C) was assigned to the reduction of PtOx and Co^{3+} to Co^{2+} cations with weak interaction with support and promoted by Pt; the peak at 331 °C was ascribed to the reduction of Co^{3+} species in close interaction with the support. The prominent peak at 563 °C was assigned to the simultaneous reduction of Co^{2+} species from cobalt oxide spinel and a fraction of the Co^{2+} ions in the cobalt aluminate [36]. In the subsequent $TPR_{600/950}$ a single peak was detected at 766 °C, which corresponded to the reduction of cobalt species in the cobalt aluminate phase. The TPR_{600} H_2 uptake of fresh catalyst was 5.1 $mmol_{H2}/g_{cat}$, while the H_2 uptake in the $TPR_{600/950}$ run was 2.2 $mmol_{H2}/g_{cat}$. That is, around 30% of the Co species remained oxidized after the TPR_{600} run. According to XPS data, these unreduced species were Co^{2+}, which required an extremely high reduction temperature ($TPR_{600/950}$) to be fully reduced.

Regarding the spent catalysts, the TPR_{600} profile varied depending on the feedstream employed. Since the catalyst was pre-reduced at 600 °C any hydrogen uptake band in the TPR_{600} run should be linked to metal oxidation or hydrogenation of carbonaceous compounds. H_2 uptake values varied in the 0.2–3.1 $mmol_{H2}/g_{cat}$ range (Fig. 6a, Table 3). As could be expected, the $TPR_{600/950}$ profiles of all the spent catalysts were qualitatively very similar to that from the fresh solid, with a unique main consumption band.

According to Table 3, the $TPR_{600/950}$ H_2 uptake for catalysts used in methanol and acetic acid APR was higher than that of fresh catalyst, suggesting the existence of newly formed cobalt aluminate at the interface of the metallic cobalt crystallite and alumina-rich support [73]. However, H_2-TPR data should be taken with caution since several phenomena can affect samples. The loss of metallic surface by re-deposition of aluminium hydroxide could attenuate the hydrogen spillover, and thus decrease the amount of cobalt ions as cobalt aluminate that have been reduced in the TPR_{600} run. Moreover, the extremely low TPR_{600} H_2 uptake of catalyst used in acetic acid APR could be a consequence of a lower re-oxidation but instead, it could be also associated with the high

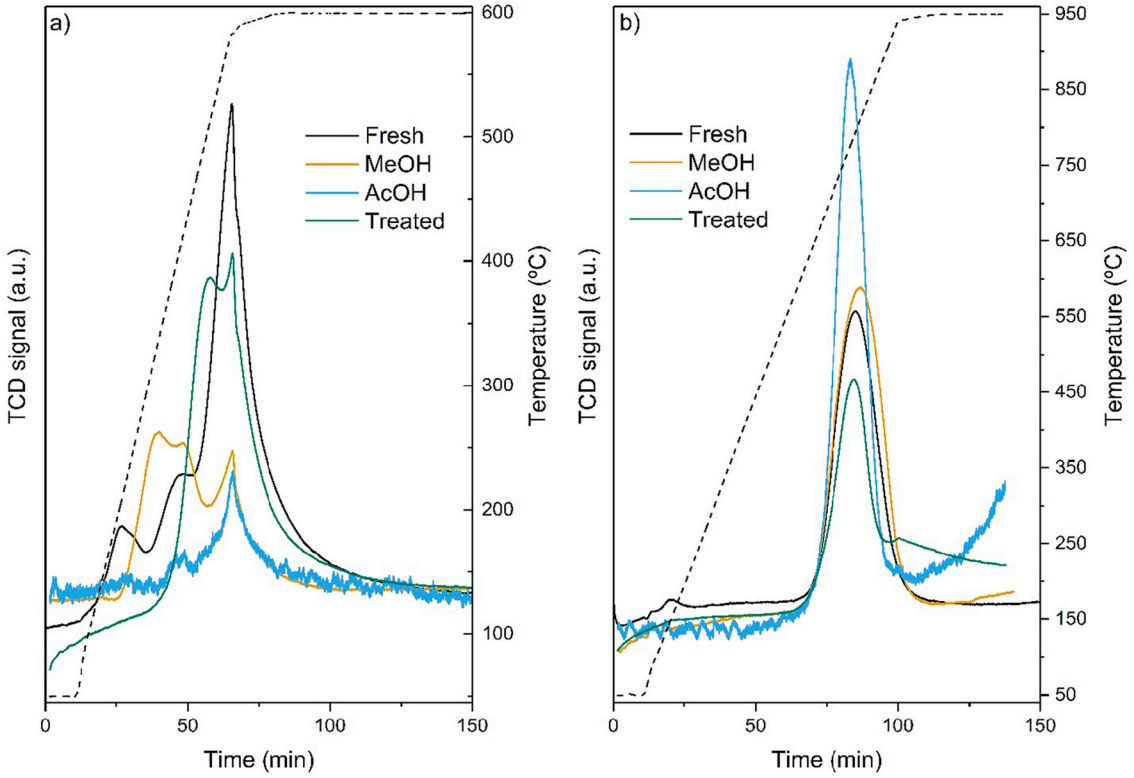

Fig. 6. Profiles of (a) TPR_{600} and (b) $TPR_{600/950}$; AcOH: acetic acid, MeOH: methanol.

percentage of leached cobalt. Indeed, re-oxidation is the first step of leaching mechanism [74].

In order to discern between the hydrogen uptake for the reduction of oxidized species and for the hydrogenation of carbonaceous deposits, TPH experiments were conducted by coupling a mass spectrometer to the reduction reactor exhaust, following the evolution of methane (m/z = 15 signal) upon heating up to 600 °C followed by an isothermal stage for 60 min (Fig. S7, Supporting Information). As expected, no methane was detected in the TPH of fresh catalyst. Contrarily, for the catalyst used in methanol APR, methane release began at 200 °C and finished at 500 °C, with a maximum at 375 °C. For the other spent catalysts, it started at around 280 °C and extended up to 600 °C. TPH signal showed several shoulders, suggesting methane formation from either hydrogenation of different substrates or at different active sites. According to the previously discussed FTIR data, the peak at the lowest temperature for the methanol APR-spent catalysts was due to hydrogenation of small molecules adsorbed into the catalysts pores. In quantitative terms, the released amount of methane (i.e. 0.13–0.24 $\mu mol_C/g_{cat}$) was significantly lower than that reported by others under similar conditions (>1.75 $\mu mol_C/g_{cat}$) [13], what is in agreement with our XRD and Raman results. Accordingly, the measured H_2 uptake in TRP_{600} could be attributed to the reduction of cobalt oxide nanoparticles (formed by re-oxidation in the aqueous-phase environment) which ranged between 4% (after acetic acid APR) and 60% (after "treated" glycerol APR). Taken into account that oxidation promotes metal leaching [75], some means of preventing the oxidation of the metallic phases would contribute to the development of cobalt catalysts with extended lifetime for aqueous-phase reaction. According to the above observations, the reduction of Co and the removal of coke could be achieved by treatment with H_2 at 500 °C, which could be done in-situ. Indeed, the reduction treatment could only partially regenerate the catalyst due to the irreversible catalyst deactivation caused by metal leaching and/or salt deposition. Alternative strategies aimed to stabilize the metal nanoparticles against leaching and more in-deep pre-treatments for removing salt precursors could hinder catalyst deactivation.

4. Conclusions

Waste glycerol from biodiesel plants has proven to be a potential feedstock for the production of energy and other valuable chemicals by means of Aqueous-Phase Reforming (APR). Firstly, the physico-chemical characteristics of crude bioglycerol (by-product waste from a local biodiesel plant) were thoroughly analyzed in order to ascertain an appropriate purification protocol. A multi-step procedure, comprising alkalization, neutralization, and filtration of the feedstock was conducted and the so-called "treated" glycerol solution was obtained. Such treatment aimed to effectively reduce the content of fatty acids, but failed to reduce the percentage of ash.

"Treated" glycerol aqueous solution was subjected to APR over 0.3Pt/CoAl catalyst covering a very wide glycerol conversion range (14.3–99.7%). It was found that the Gas to Liquid ratio of C-containing products, and the yield and selectivity to hydrogen increased with glycerol conversion, especially at conversion values above 60%. A volcano-type dependence was observed in the selectivity to alkanes, with maximum values in the X_{Gly} 30–65% range. Regarding the liquid products, hydroxyacetone, 1,2-propylene glycol and propanoic acid were the identified main products, which distribution strongly varied with X_{Gly}. Carbon selectivity to 1,2-propylene glycol (the most valuable liquid product) was maximized in the 60–90% glycerol conversion range (c.a. 16% carbon selectivity). The effect of impurities was assessed by conducting additional APR tests with methanol and acetic acid aqueous solutions. It was concluded that catalyst stability was compromised when acetic acid was present in the feedstock, where the acidity of the reaction solution might promote cobalt leaching issues. In addition, oxidation of the metallic phase and carbon deposition was observed after APR tests. The basis for the regeneration of the spent catalyst, consisting of a reductive treatment at 500 °C, has been established.

CRediT authorship contribution statement

A.J. Reynoso: Investigation, Writing – original draft. **J.L. Ayastuy:** Funding acquisition, Conceptualization, Writing – review & editing. **U. Iriarte-Velasco:** Formal analysis, Writing – review & editing. **M.A. Gutiérrez-Ortiz:** Resources, Funding acquisition, Supervision.

Declaration of Competing Interest

The authors declare that they have no known competing financial interests or personal relationships that could have appeared to influence the work reported in this paper.

Data availability

Data will be made available on request.

Acknowledgements

This research was supported by grant PID2019-106692EB-I00 funded by MCIN/AEI/10.13039/501100011033. The authors thank for technical support provided by SGIker of UPV/EHU and European funding (ERDF and ESF).

Appendix A. Supplementary data

Supplementary data to this article can be found online at https://doi.org/10.1016/j.fuproc.2022.107634.

References

[1] K. Madhu, C.L. Crago, M. Black, Can biofuels be a solution to climate change? The implications of land use change-related emissions for policy, Interface Focus. 1 (2011) 233–247, https://doi.org/10.1098/rsfs.2010.0016.
[2] M. Tabatabaei, M. Aghbashlo, M. Dehhaghi, H.K.S. Panahi, A. Mollahosseini, M. Hosseini, M.M. Soufiyan, Reactor technologies for biodiesel production and processing: a review, Prog. Energy Combust. Sci. 4 (2019) 239–303, https://doi.org/10.1016/j.pecs.2019.06.001.
[3] A.A. Abdul-Raman, H.W. Tan, B. Archina, Two-step purification of glycerol as a value added by product from the biodiesel production process, Front. Chem. 7 (2019) 774, https://doi.org/10.3389/fchem.2019.00774.
[4] N. Vivek, R. Sindhu, A. Madhavan, A.J. Anju, E. Castro, V. Faraco, A. Pandey, P. Binod, Recent advances in the production of value added chemicals and lipids utilizing biodiesel industry generated crude glycerol as a substrate-Metabolic aspects, challenges and possibilities: an overview, Bioresour. Technol. 239 (2017) 507–517, https://doi.org/10.1016/j.biortech.2017.05.056.
[5] S.C. D'Angelo, A. Dall'Ara, C. Mondelli, J. Pérez-Ramírez, S. Papadokonstantakis, Techno-Economic Analysis of a Glycerol Biorefinery, ACS Sustain. Chem. Eng. 6 (2018) 16563–16572, https://doi.org/10.1021/acssuschemeng.8b03770.
[6] T. Mizik, G. Gyarmati, Economic and Sustainability of biodiesel Production-a Systematic Literature Review, Clean Technol. 3 (2021) 19–36, https://doi.org/10.3390/cleantechnol3010002.
[7] U.I. Nda-Umar, I. Ramli, Y.H. Taufiq-Yap, E.N. Muhamad, An Overview of recent Research i n the Conversion of Glycerol into Biofuels, fuel Additives and other Bio-based Chemicals, Catalysts. 9 (2019) 15, https://doi.org/10.3390/catal9010015.
[8] M. Checa, S. Nogales-Delgado, V. Montes, J.M. Encinar, Recent advances in Glycerol Catalytic Valorization: a Review, Catalysts. 10 (2020) 1279, https://doi.org/10.3390/catal10111279.
[9] R. Cortright, R. Davda, J. Dumesic, Hydrogen from catalytic reforming of biomass-derived hydrocarbons in liquid water, Nature. 418 (2002) 964–967, https://doi.org/10.1038/nature01009.
[10] R.L. Manfro, A.F. da Costa, N.F.P. Ribeiro, M.M.V.M. Souza, Hydrogen production by aqueous-phase reforming of glycerol over nickel catalysts supported on CeO_2, Fuel Process. Technol. 92 (2011) 330–335, https://doi.org/10.1016/j.fuproc.2010.09.024.
[11] R.R. Davda, J.W. Shabaker, G.W. Huber, R.D. Cortright, J.A. Dumesic, A review of catalytic issues and process conditions for renewable hydrogen and alkanes by aqueous-phase reforming of oxygenated hydrocarbons over supported metal catalysts, Appl. Catal. B:Environ. 56 (2005) 171–186, https://doi.org/10.1016/j.apcatb.2004.04.027.
[12] U.I. Nda-Umar, I. Ramli, Y.H. Taufiq-Yap, E.N. Muhamad, An Overview of recent Research in the Conversion of Glycerol into Biofuels, fuel Additives and other Bio-based Chemicals, Catalysts 9 (2019) 15, https://doi.org/10.3390/catal9010015.

[13] A.J. Reynoso, J.L. Ayastuy, U. Iriarte-Velasco, M.A. Gutiérrez-Ortiz, Aqueous-phase reforming of glycerol over Pt-Co catalyst: effect of process variables, J. Environ. Chem. Eng. 10 (3) (2022), 107402, https://doi.org/10.1016/j.jece.2022.107402.

[14] M.M. Rahman, Aqueous-phase Reforming of Glycerol over Carbon-Nanotube-Supported Catalysts, Catal. Lett. 150 (2020) 2674–2687, https://doi.org/10.1007/s10562-020-03167-2.

[15] W. Cheng, Y. Wang, M. Chen, D. Liang, C. Li, Z. Yang, J. Wang, Hydrogen production from aqueous phase reforming of glycerol over attapulgite-supported nickel catalysts: effect of acid/base treatment and Fe additive, Int. J. Hydrogen Energ. 47 (119) (2022) 7082–7099, https://doi.org/10.1016/j.ijhydene.2021.12.082.

[16] K. Wu, B. Dou, H. Zhang, D. Liu, H. Chen, Y. Xu, Aqueous phase reforming of biodiesel byproduct glycerol over mesoporous Ni-Cu/CeO_2 for renewable hydrogen production, Fuel 308 (2022), 122014, https://doi.org/10.1016/j.fuel.2021.122014.

[17] D. Liu, B. Dou, H. Zhang, L. Zhao, K. Wu, P. Zeng, H. Chen, Y. Xu, Comparison of gelatinous and calcined magnesia supported Ni or/and Co-based catalysts for aqueous phase reforming of glycerol, Renew. Energ. 186 (2022) 656–666, https://doi.org/10.1016/j.renene.2022.01.040.

[18] I. Coronado, M. Stekrova, L. García-Moreno, M. Reinikainen, P. Simell, R. Karinen, J. Lehtonen, Aqueous-phase reforming of methanol over nickel-based catalysts for hydrogen production, Biomass Bioenergy 106 (2017) 29–37, https://doi.org/10.1016/j.biombioe.2017.08.018.

[19] Z. Xiao, Q. Meng, C. Qiu, S. Qiu, X. Wu, L. Ma, T. Wang, Promoting mechanism of alkali for aqueous phase reforming of bio-methanol towards highly efficient production of COx-free hydrogen, Fuel Process. Technol. 236 (2022), 107385, https://doi.org/10.1016/j.fuproc.2022.107385.

[20] S. Zhang, Y. Liu, M. Zhang, Y. Ma, J. Hu, Y. Qu, Sustainable production of hydrogen with high purity from methanol and water at low temperatures, Nat. Commun. 13 (2022) 5527, https://doi.org/10.1038/s41467-022-33186-z.

[21] Q. Mao, Y. Guo, X. Liu, M. Shakouri, Y. Hu, Y. Wang, Identifying the realistic catalyst for aqueous phase reforming of methanol over Pt supported by lanthanum nickel perovskite catalyst, Appl. Catal. B:Environ. 313 (2022), 121435, https://doi.org/10.1016/j.apcatb.2022.121435.

[22] A.A. Abdul Raman, H.W. Tan, A. Buthiyappan, Two-step Purification of Glycerol as a Value added by product from the biodiesel Production Process, Front. Chem. 7 (2019) 774, https://doi.org/10.3389/fchem.2019.00774.

[23] D.J.M. de Vlieger, L. Lefferts, K. Seshan, Ru decorated carbon nanotubes - a promising catalyst for reforming bio-based acetic acid in the aqueous phase, Green Chem. 16 (2014) 864–874, https://doi.org/10.1039/C3GC41922C.

[24] J. Justicia, J.A. Baeza, A.S. Oliveira, L. Calvo, F. Heras, M.A. Gilarranz, Aqueous-phase reforming of water-soluble compounds from pyrolysis bio-oils, Renew. Energ. 199 (2022) 895–907, https://doi.org/10.1016/j.renene.2022.09.021.

[25] G. Pipitone, G. Zoppi, S. Ansaloni, S. Bocchini, F.A. Deorsola, R. Pirone, S. Bensaid, Towards the sustainable hydrogen production by catalytic conversion of C-laden biorefinery aqueous streams, Chem. Eng. J. 377 (2019), 120677, https://doi.org/10.1016/j.cej.2018.12.137.

[26] A. Arandia, I. Coronado, A. Remiro, A.G. Gayubo, M. Reinikainen, Aqueous-phase reforming of bio-oil aqueous fraction over nickel-based catalysts, Int. J. Hydrogen Energ. 44 (26) (2019) 13157–13168, https://doi.org/10.1016/j.ijhydene.2019.04.007.

[27] P. Lozano, A.I. Simón, L. García, J. Ruiz, M. Oliva, J. Arauzo, Influence of the Ni-Co/Al-Mg catalyst loading in the continuous aqueous phase reforming of the bio-oil aqueous fraction, Processes 9 (2021) 81, https://doi.org/10.3390/pr9010081.

[28] F. Héroguel, B. Rozmysłowicz, J.S. Luterbacher, Improving Heterogeneous Catalyst Stability for Liquid-phase Biomass Conversion and Reforming, Chimia. 69 (2015) 582–591, https://doi.org/10.2533/chimia.2015.582.

[29] K. Wu, B. Dou, H. Zhang, D. Liu, H. Chen, Y. Xu, Effect of impurities of CH_3OH, CH_3COOH, and KOH on aqueous phase reforming of glycerol over mesoporous Ni–Cu/CeO_2 catalyst, J. Energy Inst. 99 (2021) 198–208, https://doi.org/10.1016/j.joei.2021.09.009.

[30] G. Zoppi, G. Pipitone, R. Pirone, S. Bensaid, Aqueous phase reforming process for the valorization of wastewater streams: Application to different industrial scenarios, Catal. Today 387 (2022) 224–236, https://doi.org/10.1016/j.cattod.2021.06.002.

[31] D.A. Boga, F. Liu, P.C.A. Bruijnincx, B.M. Weckhuysen, Aqueous-phase reforming of crude glycerol: effect of impurities on hydrogen production, Catal. Sci. Technol. 6 (2016) 134–143, https://doi.org/10.1039/C4CY01711K.

[32] K. Lehnert, P. Claus, Influence of Pt particle size and support type on the aqueous-phase reforming of glycerol, Catal. Comm. 9 (2008) 2543–2546, https://doi.org/10.1016/j.catcom.2008.07.002.

[33] A. Larimi, F. Khorasheh, Renewable hydrogen production over Pt/Al_2O_3 nano-catalysts: effect of M-promoting (M=Pd, Rh, Re, Ru, Ir, Cr), Int. J. Hydrogen Energ. 44 (2019) 8243–8251, https://doi.org/10.1016/j.ijhydene.2019.01.251.

[34] J. Remón, J. Ruiz, M. Oliva, L. García, J. Arauzo, Effect of biodiesel-derived impurities (acetic acid, methanol and potassium hydroxide) on the aqueous phase reforming of glycerol, Chem. Eng. J. 299 (2016) 431–448, https://doi.org/10.1016/j.cej.2016.05.018.

[35] J. Remón, C. Jarauta-Córdoba, L. García, J. Arauzo, Effect of acid (CH_3COOH, H_2SO_4 and H_3PO_4) and basic (KOH and NaOH) impurities on glycerol valorisation by aqueous phase reforming, Appl. Catal. B:Environ. 219 (2017) 362–371, https://doi.org/10.1016/j.apcatb.2017.07.068.

[36] A.J. Reynoso, U. Iriarte-Velasco, M.A. Gutiérrez-Ortiz, J.L. Ayastuy, Highly stable Pt/$CoAl_2O_4$ catalysts in Aqueous-phase Reforming of glycerol, Catal. Today 367 (2021) 278–289, https://doi.org/10.1016/j.cattod.2020.03.039.

[37] S. Hu, X. Luo, C. Wan, Y. Li, Characterization of Crude Glycerol from biodiesel Plants, J. Agric. Food Chem. 60 (23) (2012) 5915–5921, https://doi.org/10.1021/jf3008629.

[38] Glycerols for industrial use-Determination of ash-Gravimetric method, ISO 2098 (1972).

[39] M. García-Diéguez, D.D. Hibbitts, E. Iglesia, Hydrogen Chemisorption Isotherms on platinum Particles at Catalytic Temperatures: Langmuir and Two-Dimensional Gas Models Revisited, J. Phys. Chem. C 123 (13) (2019) 8447–8462, https://doi.org/10.1021/acs.jpcc.8b10877.

[40] L.R. Kumar, S.K. Yellapu, R.D. Tyagi, X. Zhang, A review on variation in crude glycerol composition, bio-valorization of crude and purified glycerol as carbon source for lipid production, Bioresour. Technol. 293 (2019), 122155, https://doi.org/10.1016/j.biortech.2019.122155.

[41] M. Kachel-Jakubowska, A. Matwijczuk, M. Gagoś, Analysis of the physicochemical properties of post-manufacturing waste derived from production of methyl esters from rapeseed oil, Int. Agrophys. 175-182 (2017), https://doi.org/10.1515/intag-2016-0042.

[42] S.R.M. Kollar, E.H. Novotny, C.J. Do Nascimento, P.A.Z. Suarez, Nuclear magnetic Resonance (1.40 T) and Mid infrared (FTIR-ATR) Associated with Chemometrics as Analytical Methods for the Analysis of Methyl Ester Yield Obtained by Esterification Reaction, J. Braz. Chem. Soc. 28 (2017) 1917–1925, https://doi.org/10.21577/0103-5053.20170031.

[43] I. Doroshenko, V. Pogorelov, V. Sablinskas, Infrared Absorption Spectra of Monohydric Alcohols, Dataset Papers in Science, Article ID 329406 (2013), https://doi.org/10.7167/2013/329406.

[44] N.N. Mahamuni, Y.G. Adewuyi, Fourier Transform infrared Spectroscopy (FTIR) Method to Monitor Soy biodiesel and soybean Oil in Transesterification Reactions, Petrodiesel−biodiesel Blends, and Blend Adulteration with Soy Oil, Energy Fuel 23 (7) (2009) 3773–3782, https://doi.org/10.1021/ef900130m.

[45] J.A. Heredia-Guerrero, J.J. Benítez, P. Cataldi, U.C. Paul, M. Contardi, R. Cingolani, I.S. Bayer, A. Heredia, A. Athanassiou, All-Natural Sustainable packaging Materials inspired by Plant Cuticles, Adv. Sustainable Syst. 1 (2017) 1600024(9), https://doi.org/10.1002/adsu.201600024.

[46] L. García, A. Valiente, M. Oliva, J. Ruiz, J. Arauzo, Influence of operating variables on the aqueous-phase reforming of glycerol over a Ni/Al coprecipitated catalyst, Int. J. Hydrogen Energ. 43 (2018) 20392–20407, https://doi.org/10.1016/j.ijhydene.2018.09.119.

[47] H.D. Kim, H.J. Park, T.W. Kim, K.E. Jeong, H.J. Chae, S.Y. Jeong, C.H. Lee, C. U. Kim, The effect of support and reaction conditions on aqueous phase reforming of polyol over supported Pt–Re bimetallic catalysts, Catal. Today 185 (2012) 73–80, https://doi.org/10.1016/j.cattod.2011.08.012.

[48] P.J. Dietrich, M.C. Akatay, F.G. Sollberger, E.A. Stach, J.T. Miller, W.N. Delgass, F. H. Ribeiro, Effect of Co Loading on the activity and Selectivity of PtCo Aqueous phase Reforming Catalysts, ACS Catal. 4 (2) (2014) 480–491, https://doi.org/10.1021/cs4008705.

[49] A.J. Reynoso, J.L. Ayastuy, U. Iriarte-Velasco, M.A. Gutiérrez-Ortiz, Bimetallic Pt-Co Catalysts for the Liquid-phase WGS, Catalysts 10 (2020) 830, https://doi.org/10.3390/catal10080830.

[50] M.F.N. D'Angelo, V. Ordomsky, J. van der Schaaf, J.C. Schouten, T.A. Nijhuis, Continuous hydrogen stripping during aqueous phase reforming of sorbitol in a washcoated microchannel reactor with a Pt–Ru bimetallic catalyst, Int. J. Hydrogen Energ. 39 (2014) 18069–18076, https://doi.org/10.1016/j.ijhydene.2014.02.167.

[51] J.W. Shabaker, J.A. Dumesic, Kinetics of Aqueous-phase Reforming of Oxygenated Hydrocarbons: Pt/Al_2O_3 and Sn-Modified Ni Catalysts, Ind. Eng. Chem. Res. 43 (12) (2004) 3105–3112, https://doi.org/10.1021/ie049852o.

[52] T. Nozawa, Y. Mizukoshi, A. Yoshida, S. Naito, Aqueous phase reforming of ethanol and acetic acid over TiO_2 supported Ru catalysts, Appl. Catal. B:Environ. 146 (2014) 221–226, https://doi.org/10.1016/j.apcatb.2013.06.017.

[53] D. Li, Y. Li, X. Liu, Y. Guo, C.W. Pao, J.L. Chen, Y. Hu, Y. Wang, $NiAl_2O_4$ Spinel Supported Pt Catalyst: High Performance and Origin in Aqueous-phase Reforming of Methanol, ACS Catal. 9 (10) (2019) 9671–9682, https://doi.org/10.1021/acscatal.9b02243.

[54] J.W. Shabaker, R.R. Davda, G.W. Huber, R.D. Cortright, J.A. Dumesic, Aqueous-phase reforming of methanol and ethylene glycol over alumina-supported platinum catalysts, J. Catal. 215 (2) (2003) 344–352, https://doi.org/10.1016/S0021-9517(03)00032-0.

[55] Z. Tang, J. Monroe, J. Dong, T. Nenoff, D. Weinkauf, Platinum-Loaded NaY Zeolite for Aqueous-phase Reforming of Methanol and Ethanol to Hydrogen, Ind. Eng. Chem. Res. 48 (5) (2009) 2728–2733, https://doi.org/10.1021/ie801222f.

[56] P. Lakhtaria, P. Ribeirinha, W. Huhtinen, S. Viik, J. Sousa, A. Mendes, Hydrogen production via aqueous-phase reforming for high-temperature proton exchange membrane fuel cells - a review, Open Res. Europe. 1 (2022) 81, https://doi.org/10.12688/openreseurope.13812.3.

[57] D.J.M. de Vlieger, B.L. Mojet, L. Lefferts, K. Seshan, Aqueous phase Reforming of ethylene glycol – Role of intermediates in catalyst performance, J. Catal. 292 (2012) 239–245, https://doi.org/10.1016/j.jcat.2012.05.019.

[58] G. Pipitone, G. Zoppi, S. Bocchini, A.M. Rizzo, D. Chiaramonti, R. Pirone, S. Bensaid, Aqueous phase reforming of the residual waters derived from lignin-rich hydrothermal liquefaction: investigation of representative organic compounds and actual biorefinery streams, Catal. Today 345 (2020) 237–250, https://doi.org/10.1016/j.cattod.2019.09.040.

[59] M.R. Nanda, Z. Yuan, W. Qin, M.A. Poirier, X. Chunbao, Purification of Crude Glycerol using Acidification: Effects of Acid Types and Product Characterization, Austin J. Chem. Eng. 1 (1) (2014) 1004.

[60] S.N. Delgado, D. Yap, L. Vivier, C. Especel, Influence of the nature of the support on the catalytic properties of Pt-based catalysts for hydrogenolysis of glycerol, J. Mol. Catal. A:Chem. 367 (2013) 89–98, https://doi.org/10.1016/j.molcata.2012.11.001.

[61] S. Chanklang, W. Mondach, P. Somchuea, T. Witoon, M. Chareonpanich, K. Faungnawakij, A. Seubsai, Hydrogenolysis of glycerol to 1,3-propanediol over H-ZSM-5-supported iridium and rhenium oxide catalysts, Catal. Today 397–399 (2022) 356–364, https://doi.org/10.1016/j.cattod.2021.08.014.

[62] S.A. D'Ippolito, L. Pirault-Roy, C. Especel, F. Epron, C.L. Pieck, Influence of rhodium content on the behavior of Rh/SiO_2–Al_2O_3 catalysts for selective ring opening of decalin, RSC Adv. 7 (2017) 46803–46811, https://doi.org/10.1039/C7RA08350E.

[63] B. Hu, W.G. Kim, T.P. Sulmonetti, M.L. Sarazen, S. Tan, J. So, Y. Liu, R.S. Dixit, S. Nair, C.W. Jones, A Mesoporous Cobalt Aluminate Spinel Catalyst for Nonoxidative Propane Dehydrogenation, ChemCatChem 9 (2017) 3330–3337, https://doi.org/10.1002/cctc.201700647.

[64] L. Lukashuk, K. Föttinger, E. Kolar, C. Rameshan, D. Teschner, M. Hävecker, A. Knop-Gericke, N. Yigit, H. Li, E. McDermott, M. Stöger-Pollach, G. Rupprechter, Operando XAS and NAP-XPS studies of preferential CO oxidation on Co_3O_4 and CeO_2-Co_3O_4 catalysts, J. Catal. 344 (2016) 1–15, https://doi.org/10.1016/j.jcat.2016.09.002.

[65] C.E. Moffitt, B. Chen, D.M. Wieliczka, M.B. Kruger, XPS comparison between nanocrystalline γ-alumina and a new high pressure polymorph, Solid State Commun. 116 (11) (2000) 631–636, https://doi.org/10.1016/S0038-1098(00)00367-7.

[66] S. Kannan, C.S. Swamy, Catalytic decomposition of nitrous oxide over calcined cobalt aluminum hydrotalcites, Catal. Today 53 (4) (1999) 725–737, https://doi.org/10.1016/S0920-5861(99)00159-5.

[67] R.M. Ravenelle, J.R. Copeland, W.G. Kim, J.C. Crittenden, C. Sievers, Structural changes of γ-Al_2O_3-Supported Catalysts in Hot Liquid Water, ACS Catal. 1 (5) (2011) 552–561, https://doi.org/10.1021/cs1001515.

[68] L.A. Dosso, C.R. Vera, J.M. Grau, Pt-Co and Pt-Ni Catalysts of Low Metal Content for H_2 production by Reforming of Oxygenated Hydrocarbons and Comparison with Reported Pt-based Catalysts, Int. J. Chem. Eng. 4972070 (2018), https://doi.org/10.1155/2018/4972070.

[69] N.M. Eagan, J.P. Chada, A.M. Wittrig, J.S. Buchanan, J.A. Dumesic, G.W. Huber, Hydrodeoxygenation of Sorbitol to Monofunctional fuel Precursors over Co/TiO_2, Joule 1 (1) (2017) 178–199, https://doi.org/10.1016/j.joule.2017.07.004.

[70] I. Mindru, G. Marinescu, D. Gingasu, L. Patron, C. Ghica, M. Giurginca, Blue CoAl2O4 spinel via complexation method, Mater. Chem. Phys. 122 (2–3) (2010) 491–497, https://doi.org/10.1016/j.matchemphys.2010.03.032.

[71] A.V. Radha, L. Lander, G. Rousse, J.M. Tarascon, A. Navrotsky, Thermodynamic stability and correlation with synthesis conditions, structure and phase transformations in orthorhombic and monoclinic $Li_2M(SO_4)_2$ (M = Mn, Fe, Co, Ni) polymorphs, J. Mater. Chem. A 3 (2014) 2601–2608, https://doi.org/10.1039/C4TA05066E.

[72] B. Zou, S. Ren, X.P. Ye, Glycerol Dehydration to Acrolein Catalyzed by ZSM-5 Zeolite in Supercritical Carbon Dioxide Medium, ChemSusChem 9 (2016) 3268–3271, https://doi.org/10.1002/cssc.201601020.

[73] M. Wolf, N. Fischer, M. Claeys, Water-induced deactivation of cobalt-based Fischer–Tropsch catalysts, Nat. Catal. 3 (2020) 962–965, https://doi.org/10.1038/s41929-020-00534-5.

[74] T. van Haasterecht, M. Swart, K.P. de Jong, J.H. Bitter, Effect of initial nickel particle size on stability of nickel catalysts for aqueous phase reforming, J. Energy Chem. 25 (2) (2016) 289–296, https://doi.org/10.1016/j.jechem.2016.01.006.

[75] T. van Haasterecht, C.C.I. Ludding, K.P. de Jong, J.H. Bitter, Stability and activity of carbon nanofiber-supported catalysts in the aqueous phase reforming of ethylene glycol, J. Energy Chem. 22 (2) (2013) 257–269, https://doi.org/10.1016/S2095-4956(13)60032-7.